Inorg. Chem. **2006**, *45*, 189–195

Tuning the Photoinduced O_2-Evolving Reactivity of $Mn_4O_4^{7+}$, $Mn_4O_4^{6+}$, and $Mn_4O_3(OH)^{6+}$ Manganese–Oxo Cubane Complexes

Jian-Zhong Wu,[†,#] Filippo De Angelis,[†,‡] Thomas G. Carrell,[†] Glenn P. A. Yap,[§] John Sheats,[||] Roberto Car,[†] and G. Charles Dismukes*[,†]

Departments of Chemistry, Princeton University, Princeton, New Jersey 08544, University of Delaware, Newark, Delaware 19716, Rider University, Lawrenceville, New Jersey 08648, and Istituto CNR di Scienze e Tecnologie Molecolari (ISTM), c/o Dipartimento di Chimica, Università di Perugia, Via Elce di Sotto 8, I-06123 Perugia, Italy

Received September 15, 2005

The manganese–oxo "cubane" core complex $Mn_4O_4L^1_6$ (**1**, $L^1 = Ph_2PO_2^-$), a partial model of the photosynthetic water oxidation site, was shown previously to undergo photodissociation in the gas phase by releasing one phosphinate anion, an O_2 molecule, and the intact butterfly core cation ($Mn_4O_2L^1_5{}^+$). Herein, we investigate the photochemistry and electronic structure of a series of manganese–oxo cubane complexes: $[Mn_4O_4L^2_6]$ (**2**), $\mathbf{1}^+(ClO_4^-)$, $\mathbf{2}^+(ClO_4^-)$, and $Mn_4O_3(OH)L^1_6$ (**1H**). We report the atomic structure of $[Mn_4O_4L^2_6](ClO_4)$, $\mathbf{2}^+(ClO_4^-)$ [$L^2 = (4\text{-MeOPh})_2PO_2^-$]. UV photoexcitation of a charge-transfer band dissociates one phosphinate, two core oxygen atoms, and the $Mn_4O_2L_5^+$ butterfly as the dominant (or exclusive) photoreaction of all cubane derivatives in the gas phase, with relative yields: **1H** ≫ **2** > **1** > $\mathbf{2}^+$ > $\mathbf{1}^+$. The photodissociation yield increases upon (1) reducing the core oxidation state by hydrogenation of a corner oxo (**1H**), (2) increasing the electron donation from the phosphinate ligand (L^2), and (3) reducing the net charge from +1 to 0. The experimental Mn–O bond lengths and Mn–O bond strengths and the calculated ligand binding energy explain these trends in terms of weaker binding of phosphinate L^2 versus L^1 by 14.7 kcal/mol and stronger Mn–(μ_3-O)(core) bonds in the oxidized complexes $\mathbf{2}^+$ and $\mathbf{1}^+$ versus **2** and **1**. The calculated electronic structure accounts for these trends in terms of the binding energy and *antibonding* Mn–O(core) and Mn–O′(ligand) character of the degenerate highest occupied molecular orbital (HOMO), including (1) energetic destabilization of the HOMO of **2** relative to **1** by 0.75 eV and (2) depopulation of the *antibonding* HOMO and increased ionic binding in $\mathbf{1}^+$ and $\mathbf{2}^+$ versus **1** and **2**.

Introduction

Scientists and visionaries[1] have long imagined using water as a source of H_2 fuel. The photosynthetic water-oxidizing enzyme is nature's "blueprint" for designing abiotic catalysts that could oxidize water. Photosynthetic oxygen production is catalyzed by an inorganic core, $Mn_4O_xCaCl_y(HCO_3)_z$, bound within a subdomain of the photosystem II (PSII) reaction center called the water-oxidizing complex (WOC). This inorganic core is present in all oxygenic phototrophs examined so far and thus appears to be nature's universally selected catalyst for oxidizing water, refined over 2.6−3.8 billion years of evolution.[2−4] Although the atomic structure of the core is still debated,[5−9] both spectroscopic[8,10,11] and X-ray diffraction (XRD)[5,12,13] data have constrained the

* To whom correspondence should be addressed. E-mail: dismukes@princeton.edu. Phone: (609) 258-3949. Fax: (609) 258-1980.
[†] Princeton University.
[#] Present address: South China Normal University.
[‡] Università di Perugia.
[§] University of Delaware.
[||] Rider University.

(1) Verne, J. *l'sle Mysthrieuse*; Hetzel: Paris, 1874.
(2) Blankenship, R. E.; Hartman, H. *Trends Biochem. Sci.* **1998**, *23*, 94.
(3) Dismukes, G. C.; Klimov, V. V.; Baranov, S. V.; Kozlov, Y. N.; Dasgupta, J.; Tyryshkin, A. M. *PNAS—USA* **2001**, *98* (5), 2170.
(4) Olson, J. M. *Photosynth. Res.* **2001**, 68.
(5) Barber, J.; Ferreira, K.; Maghlaoui, K.; Iwata, S. *Phys. Chem. Chem. Phys.* **2004**, *6*, 4737.
(6) McEvoy, J. P.; Brudvig, G. W. *Phys. Chem. Chem. Phys.* **2004**, *6*, 4754.
(7) Dasgupta, J.; vanWilligen, R. T.; Dismukes, G. C. *Phys. Chem. Chem. Phys.* **2004**, *6*, 4793.
(8) Britt, R. D.; Campbell, K. A.; Peloquin, J. M.; Gilchrist, M. L.; Aznar, C. P.; Dicus, M. M.; Robblee, J.; Messinger, J. *Biochim. Biophys. Acta* **2004**, *1655* (1−3), 158.
(9) Lundberg, M.; Siegbahn, P. E. M. *Phys. Chem. Chem. Phys.* **2004**, *6*, 4772.
(10) Carrell, T. G.; Tyryshkin, A.; Dismukes, G. C. *J. Biol. Inorg. Chem.* **2002**, *7*, 2.

10.1021/ic051587r CCC: $33.50
Published on Web 11/10/2005

Scheme 1. PSII WOC Core Structure and Postulated "Jack-in-the-Box" Mechanism of Water Oxidation Based on the Chemistry of Manganese−Oxo Complexes[7]

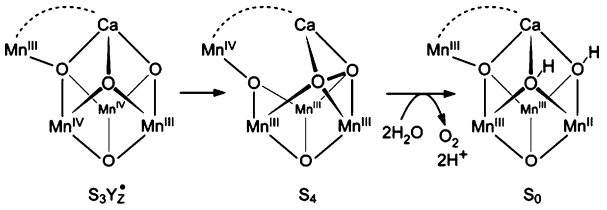

possible core topologies to only a few types. On the basis of interpretations of the available electron paramagnetic resonance (EPR), extended X-ray absorption fine structure, XRD, and Mn-reconstitution data, a leading candidate is a $CaMn_3(\mu\text{-}O)_4$ heterocubane core that is bridged to a fourth Mn at a corner μ-oxo,[7,14] as depicted in Scheme 1 (left). Four one-electron photooxidation steps (denoted S_n states, $n = 0-4$) occur that also produce structural changes involving some of the oxo bridges of the core, enroute to forming the transient S_4 state, which has yet to be characterized. Among the several postulated mechanisms for photosynthetic water splitting, the one that we favor, which is consistent with the available data to date, is depicted in Scheme 1.[7,35] This mechanism postulates that substrate water is activated for oxidation by binding to two of the core oxo sites. An all-oxo-bridged core is probably not present in the lower S states where the presence of μ-hydroxo or μ-water bridges have been implicated.[8,15]

Numerous synthetic complexes have provided insights into understanding the possible mechanisms for water oxidation and have not been restricted to manganese−oxo model complexes of the WOC.[16−19] The influence of calcium on Mn−oxo cluster properties has also begun to emerge based on both model complexes[20] and computational results.[7,9] The list of manganese complexes that are capable of water oxidation is very short, and among these, none are complete structural models of the PSII WOC. It has been well established in our laboratory that a functionally active model complex containing the symmetrical $[Mn_4O_4]^{6+}$ cubane core can be formed by spontaneous self-assembly using diarylphosphinate ligands to template formation of the $[Mn_4O_4L_6]$ molecule [L^1 = diphenylphosphinate (**1**), L^3 = ditolylphosphinate] with six facially capping ligands.[21−23] Two of the four equivalent oxygen atoms in the cubane core undergo reduction by proton-coupled electron-transfer (PCET) reaction to yield two H_2O molecules in solution (eq 1a)[22] and can also be released as molecular O_2 when triggered by photodissociation of one phosphinate ligand upon illumination in the gas phase (eq 1b). Photodissociation is quenched in condensed phases, resulting in minimal O_2 release.

$$[Mn_4O_4L_6] + 4e^- + 4H^+ \rightarrow [Mn_4O_2L_6] + 2H_2O \quad (1a)$$

$$[Mn_4O_4L_6] \leftrightarrow [Mn_4O_4L_6]^* \rightarrow [Mn_4O_2L_5]^+ + L^- + O_2 \quad (1b)$$

The goal of this research is to combine reactions such as (1a) and (1b) in a catalytic cycle, thus achieving photoinduced water oxidation in solution phase. Two approaches toward this goal examined herein are to modify the ligand or the manganese oxidation states in such a way that the barrier to O_2 release is reduced. In the first approach, using bis(4-methoxophenyl)phosphinate (L^2), we previously synthesized $[Mn_4O_4L^2_6]$ (**2**), which possesses structural, electrochemical, and electronic structural differences versus **1**.[24] In the second approach, the oxidized cubane core $[Mn_4O_4]^{7+}$ that is present in $\mathbf{1}^+$ (as both the perchlorate and triflate salts) has been previously synthesized and the XRD structure has been reported, but its photochemistry has not been studied until now. Herein we report the synthesis and physicochemical properties of $\mathbf{2}^+(ClO_4^-)$, containing the second example of the $[Mn_4O_4]^{7+}$ core. We compare the photochemical yield of the butterfly product $Mn_4O_2L_5^+$ among the series **1H**, **1**, $\mathbf{1}^+$, **2**, and $\mathbf{2}^+$, in which the core oxidation state, the capping ligand, or the hydrogenation of a corner oxo is varied. Calculations of the electronic structure and ligand binding energies (LBEs) based on density functional theory (DFT) have been applied to describe the observed ground-state properties of these complexes and their reactivity upon photoexcitation.

Experimental Section

Materials. Complexes **1**, $\mathbf{1}^+(ClO_4^-)$, and **2** were prepared as described elsewhere.[16,24−26] $Mn_4O_3(OH)L^1_6$ (**1H**) was synthesized by reduction of $\mathbf{1}^+(ClO_4^-)$ with phenothiazine (pzH) and isolated from $pz^+(ClO_4^-)$ by recrystallization, as previously described.[25] $\mathbf{2}^+(ClO_4^-)$ was synthesized similarly to $\mathbf{1}^+(ClO_4^-)$ by air oxidation of **2** in the presence of $HClO_4$. The yield of the reaction is quantitative. Single crystals of $\mathbf{2}^+(ClO_4^-)\cdot$MeCN were obtained from an acetonitrile/benzene solution.

Instrumentation. UV−vis spectra were measured on an HP-8452A diode array spectrophotometer using quartz cuvettes with a 1.0-cm path length. ^{1}H NMR spectra were obtained on a Varian INOVA 400-MHz spectrometer. Infrared spectra were measured on a Nicolet 730 Fourier transform infrared (FTIR) spectrometer,

(11) Sauer, K.; Yachandra, V. K. *Biochim. Biophys. Acta* **2004**, *1655* (1−3), 140.
(12) Biesiadka, J.; Loll, B.; Kern, J.; Irrgang, K.-D.; Zouni, A. *Phys. Chem. Chem. Phys.* **2004**, *6*, 4733.
(13) Kamiya, N.; Shen, J.-R. *PNAS−USA* **2003**, *100*, 98.
(14) Ferreira, K. N.; Iverson, T. M.; Maghlaoui, K.; Barber, J.; Iwata, S. *Science* **2004**, *303*, 1831.
(15) Haumann, M.; Muller, C.; Liebisch, P.; Iuzzolino, L.; Dittmer, J.; Grabolle, M.; Neisius, T.; Meyer-Klaucke, W.; Dau, H. *Biochemistry* **2005**, *44* (6), 1894.
(16) Ruettinger, W. F.; Ho, D. M.; Dismukes, G. C. *Inorg. Chem.* **1999**, *38* (6), 1036.
(17) Yagi, M.; Kaneko, M. *Chem. Rev.* **2001**, *101*, 21.
(18) Limburg, J.; Vrettos, J. S.; Chen, H.; de Paula, J. C.; Crabtree, R. H.; Brudvig, G. W. *J. Am. Chem. Soc.* **2001**, *123* (3), 423.
(19) Shimazaki, Y.; Nagano, T.; Takesue, H.; Ye, B.-H.; Tani, F.; Naruta, Y. *Angew. Chem., Int. Ed.* **2004**, *43*, 98.
(20) Mishra, A.; Wernsdorfer, W.; Abboud, K. A.; Christou, G. *Chem. Commun.* **2005**, 54.
(21) Ruettinger, W. F.; Yagi, M.; Wolf, K.; Bernasek, S.; Dismukes, G. C. *J. Am. Chem. Soc.* **2000**, *122*, 10353.
(22) Ruettinger, W. F.; Dismukes, G. C. *Inorg. Chem.* **2000**, *39*, 1021; correction **2000**, *39*, 4186.
(23) Yagi, M.; Wolf, K. V.; Baesjou, P. J.; Bernasek, S. L.; Dismukes, G. C. *Angew. Chem., Int. Ed.* **2001**, *40*, 2925.
(24) Wu, J.-Z.; Sellitto, E.; Yap, G. P. A.; Sheats, J.; Dismukes, G. C. *Inorg. Chem.* **2004**, *43*, 5795.
(25) Carrell, T. G.; Bourles, E.; Lin, M.; Dismukes, G. C. *Inorg. Chem.* **2003**, *42*, 2849.
(26) Carrell, T. G.; Cohen, S.; Dismukes, G. C. *J. Mol. Catal. A: Chem.* **2002**, *187*, 3.

using KBr pellets. EPR spectra were recorded at 9.5 GHz on a Bruker ESP300 spectrometer equipped with Oxford cryostat model 900. Laser-desorption ionization mass spectroscopy (LDI-MS) was conducted by vaporization and ionization of the solid compound on a gold surface using a pulsed N_2 laser (337 nm, 1 ns duration, microjoule energies) to excite the UV absorption band under vacuum (order of 10^{-7} Torr), as previously described.[21,23]

XRD Data Collection and Structure Determination. XRD data were collected on a Siemens-AXS APEX diffractometer with Mo Kα radiation ($\lambda = 0.710\ 73$ Å) at $T = 120$ K. Direct methods were used with multiabsorption correction and full-matrix refinement. Non-hydrogen atoms were refined anisotropically with hydrogen atoms in calculated positions. Scattering factors were obtained from the SHELXTL 6.12 program library (G. M. Sheldrick, Madison, WI, 2001): $C_{84}H_{84}ClMn_4O_{32}P_6$?$C_2H_3N$, fw = 2088.60, triclinic, $P1$, $a = 15.457(2)$ Å, $b = 15.921(2)$ Å, $c = 20.663(3)$ Å, $\alpha = 109.559(2)°$, $\beta = 110.055(2)°$, $\gamma = 99.131(3)°$, $V = 4456.7(12)$ Å^3, $Z = 2$, $\rho_{calcd} = 1.556$ g cm^{-1}, $\theta_{max} = 28.28°$, 19 912 observed unique reflections ($I_o > 2\sigma I_o$), $T_{min}/T_{max} = 0.9846/0.7835$, $\mu = 0.777$ mm^{-1}, R1 = 0.0606, wR2 = 0.1376, GOF = 1.067. CIF deposited with Cambridge Crystallographic Data Centre as CCDC 275067.

Computational Details. First, the geometry of complex **1** was optimized under tetrahedral (T_d) symmetry constraints using the ADF program package,[27,28] together with the BPW91 exchange-correlation functional[29,30] and a standard TZP basis set for Mn and a DZP basis set for O, P, C, and H atoms. For computational convenience, we considered a closed-shell ground-state wave function for geometry optimizations. The calculated Mn−O(core), Mn−O(phosphinate), and Mn−Mn distances (1.92, 1.93, and 2.96 Å, respectively) are in good agreement with experimental XRD data despite the neglect of spin-polarization in the geometry optimization. Next, for complex **2**, we fixed the geometry to that optimized for complex **1** and replaced the para H atoms in the phenyl rings of the $Ph_2PO_2^-$ ligands by MeO− groups, so as to disentangle electronic structure factors related to replacing the ligands from geometrical variations within the cubane core. The geometrical parameters of the MeO− groups were obtained from a separate geometry optimization of the MeOPh species at the same level of theory used for the optimization of complex **1**. We then performed a spin-polarized calculation for the $S = 7$ spin states of complexes **1** and **2**. At this stage, the B3LYP exchange-correlation functional was used,[31] as implemented in the *Gaussian03* (G03) program package.[32] A standard 3-21G* basis set was used for Mn, O, and P atoms, while for the C and H atoms, the unpolarized 3-21G basis set was used. The same level of theory was used to evaluate LBEs. LBEs are defined as follows:

$$\mathrm{LBE[L]} = E[\mathrm{Mn_4O_4L_6}] - E[\mathrm{Mn_4O_4L_5^+}] - E[\mathrm{L^-}]$$

where L^- is $Ph_2PO_2^-$ (L^1) or $(4\text{-MeOPh})_2PO_2^-$ (L^2). LBEs were evaluated using an approximate procedure in which no geometry relaxations were performed. Because of this limitation, only relative LBEs are meaningful.

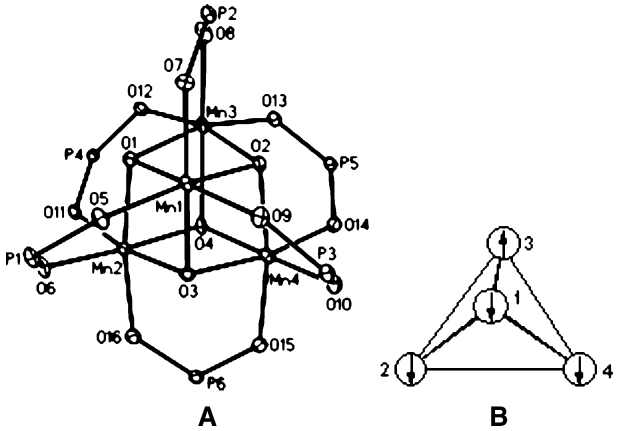

Figure 1. (left) ORTEP view (50% probability) of $\mathbf{2}^+(ClO_4^-)$ with anisole rings omitted for clarity. Selected distances (Å): Mn1−Mn2, 2.8503(8); Mn1−Mn3, 2.8950(8); Mn1−Mn4, 2.8339(7); Mn2−Mn3, 2.9318(7); Mn2−Mn4, 2.8450(7); Mn3−Mn4, 2.9549(8); Mn1−O7, 1.877(2); Mn1−O1, 1.880(2); Mn1−O3, 1.889(2); Mn1−O2, 1.890(2); Mn1−O9, 1.908-(2); Mn1−O5, 1.910(2); Mn2−O4, 1.860(2); Mn2−O11, 1.897(2); Mn2−O6, 1.909(2); Mn2−O3, 1.911(2); Mn2−O1, 1.914(2); Mn2−O16, 1.933(2); Mn3−O12, 1.904(2); Mn3−O13, 1.936(2); Mn3−O2, 1.938(2); Mn3−O1, 1.958(2); Mn3−O8, 2.007(3); Mn3−O4, 2.094(2); Mn4−O4, 1.894(2); Mn4−O15, 1.898(2); Mn4−O2, 1.901(2); Mn4−O3, 1.909(2); Mn4−O14, 1.921(2); Mn4−O10, 1.923(2). (right) Predicted magnetic spin topology for the $S = {}^5/_2$ intermediate-spin ground state of $\mathbf{2}^+(ClO_4^-)$ based on a Heisenberg exchange coupling model with Mn^{III}(3) and three Mn^{IV}(1,2,4).

Results and Discussion

The crystal structures of the two neutral cubanes differ by transition from a tetrahedral Mn_4O_4 core in **1** with identical Mn sites to C_{2v} point symmetry in **2** with pairs of discrete Mn^{III} and Mn^{IV} sites.[24] For this reason, we were also interested in their corresponding cations. The crystal structure of $\mathbf{2}^+(ClO_4^-)$ with the anisole rings and perchlorate anion omitted is shown in Figure 1A. The six Mn−Mn distances exhibit approximate trigonal symmetry. Mn3 forms the apex of the trigonal prism with longer Mn3−Mn1, −Mn2, or −Mn4 distances than those within the base of the prism by 0.084 Å (average). In this respect, it is similar to the core of $\mathbf{1}^+$.[16] Minor contraction of the trigonal prism along the Mn1−Mn3 axis lowers the effective core symmetry to nearly C_{2v}. Mn1, Mn2, and Mn4, which form the base of the trigonal pyramid have no Jahn−Teller distortions. By contrast, Mn3 shows an obvious Jahn−Teller elongation along the O4−Mn3−O8 axis, with Mn3−O4 and Mn3−O8 lengths both above 2 Å (average 2.051 Å), whereas the four equatorial Mn3−O bonds are all below 2 Å (average 1.934 Å). A local Mn−O Jahn−Teller distortion was not observed for the trigonal complex $\mathbf{1}^+$,[16] although this Jahn−Teller distortion is smaller ($\Delta R = 0.117$ Å) than that observed in the neutral complex **2** ($\Delta R = 0.227$ Å).[24] Thus, the apical Mn3 can be assigned as Mn^{III}, and the other three Mn atoms are in the 4+ oxidation state.

The ^{1}H NMR spectrum of $\mathbf{2}^+$ in a methylene chloride solution at room temperature exhibits a single chemical shift at 3.77 ppm and intensity due to the 12 terminal methyl groups, while the phenyl protons give a single broad peak at 7.7 ppm with unresolved fine structure. Thus, $\mathbf{2}^+$ possesses tetrahedral symmetry in solution, consistent with a delocal-

(27) te Velde, G.; Bickelhaupt, F. M.; Baerends, E. J.; Fonseca Guerra, C.; van Gisbergen, S. J. A.; Snijders, J. G.; Ziegler, T. *J. Comput. Chem.* **2001**, *22*, 931.
(28) Fonseca Guerra, C.; Visser, O.; Snijders, J. G.; te Velde, G.; Baerends, E. J. *Methods and Techniques for Computational Chemistry*; STEF: Cagliari, Italy, 1995; pp 303−395.
(29) Becke, A. D. *Phys. Rev.* **1988**, *A38*, 3098.
(30) Perdew, J. P.; Wang, Y. *Phys. Rev.* **1992**, *B45*, 13244.
(31) Becke, A. D. *J. Chem. Phys.* **1993**, *98*, 5648.
(32) Frisch, M. J.; Trucks, G. W.; Schlegel, H. B.; Scuseria, G. E.; Robb, M. A.; Cheeseman, J. R.; Montgomery, J. A.; Vreven, T.; Kudin, K. N.; Burant, J. C.; et al. *Gaussian 03*, revision B.05; Gaussian Inc.: Pittsburgh, PA, 2003.

ized electronic valence on the NMR time scale. This behavior is analogous to that of $\mathbf{1}^+$, which also exhibits a transition from localized to delocalized valence upon dissolution of the crystal phase.

The ^{1}H NMR resonances of both the *p*-methyl and aromatic hydrogens of $\mathbf{2}^+$ are only weakly shifted upfield ($\leq$0.5 ppm) compared to those of both **2** and the free ligand, indicating that there is little transfer of unpaired spin density into the carbon framework of the aryl rings. FTIR spectroscopy of $\mathbf{2}^+$ reveals that the phosphinate O−P−O symmetric stretching vibration at 964 cm^{-1} decreases by 23 cm^{-1} relative to **2**,[24] indicating weaker P−O bonding. This decreased P−O bond strength correlates with stronger Mn−O(L^2) bonding in $\mathbf{2}^+$ versus **2**, as determined by the shorter bond lengths, 0.046 Å shorter in $\mathbf{2}^+$ than in **2** on average (1.9184 and 1.9642 Å, respectively), while the P−O bonds are correspondingly longer by 0.008 Å (average 1.5385 and 1.5308 Å, respectively).

This increase in binding affinity between the $[Mn_4O_4]^{7+}$ core and the L^2 phosphinate ligand is also evident in the electrochemical properties. The $\mathbf{2}^+/\mathbf{2}$ reduction couple is shifted down appreciably by ca. 150 mV relative to $\mathbf{1}^+/\mathbf{1}$,[24] indicating greater stabilization of the oxidized core by the L^2 ligand relative to L^1. This shift provides direct experimental proof of greater electron donation by L^2 into the $[Mn_4O_4]^{7+}$ core.

Variable-temperature EPR (at 9 GHz) of a frozen solution of $\mathbf{2}^+$ reveals that it possesses a paramagnetic ground state that is identical with that found in $\mathbf{1}^+$.[16] Fine structure peaks are resolved at effective *g* values of 7.0, 4.9, 3.3, 2.9, and 2.0, with only the latter transition exhibiting a derivative line shape (see the Supporting Information). Like $\mathbf{1}^+$, these features can be attributed to the zero-field splitting of an $S = {}^5/_2$ ground state in orthorhombic symmetry.[33] An $S = {}^5/_2$ state is the expected intermediate spin ground state for an $Mn^{III}Mn^{IV}_3$ cluster in which an apical $S = 2$ Mn^{III} is antiferromagnetically coupled to all three basal $S = {}^3/_2$ ions, which are mutually ferromagnetically coupled (Figure 1B).

Matrix-free LDI-MS at 337 nm was previously used to characterize the photochemistry of solid **1** and its (μ-^{18}O)$_4$ isotopomer, revealing a high-selectivity high-yield intramolecular photodissociation reaction that produces O_2 from the corner oxos and the $L_6Mn_4O_2^+$ "butterfly" complex, as shown in eq 1b. Release of molecular O_2 was shown to occur only if one phosphinate ligand is also photodissociated, and this photodissociation was the only reaction observed other than relaxation to the ground state.[22,23] LDI-MS spectra for $\mathbf{1}^+$, **2**, and $\mathbf{2}^+$ are compared to **1** in Figure 2 at similar laser powers. The same trend is observed at all laser powers examined (see the Supporting Information). LDI-MS shows that in all of these complexes no oxygen atoms are released unless one phosphinate ligand is also photodissociated (no peaks at the parent mass minus $m/z = 16$). For **1** and $\mathbf{1}^+$, there are two main species that form, the cubane cation $[Mn_4O_4L^1{}_6]^+$ and the butterfly cation $[Mn_4O_2L^1{}_5]^+$ at m/z 1586 and 1337, respectively. The same behavior is found

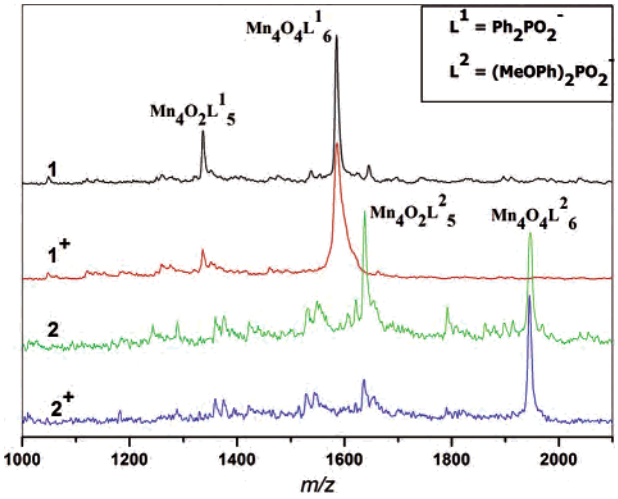

Figure 2. LDI-MS spectra (positive mode) of **1**, $\mathbf{1}^+$, **2**, and $\mathbf{2}^+$ using a N_2 laser at 337 nm. Laser power: 3.2−3.4 μJ.

Table 1. Comparison of Selected Average Bond Lengths (Å)

complex	Mn−(μ_3-O)	Mn−O(L^1 or L^2)
1	1.952	1.944
2	1.945	1.965
$\mathbf{1}^+$	1.922	1.914
$\mathbf{2}^+$	1.920	1.918

for **2** and $\mathbf{2}^+$, which yield two main cationic species $[Mn_4O_4L^2{}_6]^+$ (cubane) and $[Mn_4O_2L^2{}_5]^+$ (butterfly), which appear at m/z 1946 and 1637, respectively. Apparently the relative yield of the "butterfly" is quite different for these four complexes. The ratio of the butterfly photoproduct to the cubane (peak heights) was found to be 0.36 for **1** and decreased to be 0.22 for $\mathbf{1}^+$. This ratio increased significantly to 1.18 for **2** and to 0.30 for $\mathbf{2}^+$. So, both of the oxidized cubane complexes ($\mathbf{1}^+$ and $\mathbf{2}^+$) have reduced photoreactivity compared to their corresponding neutral cubane. This relative reduction in the photoproduct cannot be accounted for by a difference in their light absorption efficiencies because both $\mathbf{1}^+$ and $\mathbf{2}^+$ absorb light with higher molar absorptivity than do **1** and **2**, respectively, at the laser wavelength 337 nm. The UV−vis absorption spectra are given in the Supporting Information.

It is significant that **2** produces a much higher yield of the butterfly photoproduct than does **1**. This is also true for $\mathbf{2}^+$ versus $\mathbf{1}^+$, although not nearly so large an increase. These observations imply that the bis(4-methoxophenyl)phosphinate ligand photodissociates with higher probability from the cubane complex than the diphenylphosphinate ligand. This increase in the photodissociation yield can be explained by the structural data in Table 1. On going from **1** to **2**, the average Mn−(μ_3-O) bond length slightly decreases by 0.007 Å while the Mn−O(L) increases significantly by 0.02 Å, which implies that the Mn−O(L^2) coordination bond is weaker than Mn−O(L^1). This trend is also found for $\mathbf{1}^+$ and $\mathbf{2}^+$, although it is smaller.

The lower yield of the butterfly photoproduct for $\mathbf{2}^+$ and $\mathbf{1}^+$ compared to **2** and **1,** respectively, could be due to both differences in charge and Mn−O bond strength. As is evident by the structural data in Table 1, $\mathbf{1}^+$ and $\mathbf{2}^+$ both have shorter Mn−O(L) and Mn−(μ_3-O)(core) bonds compared to **1** and

(33) Weltner, W. *Magnetic Atoms and Molecules*; Dover: New York, 1983.

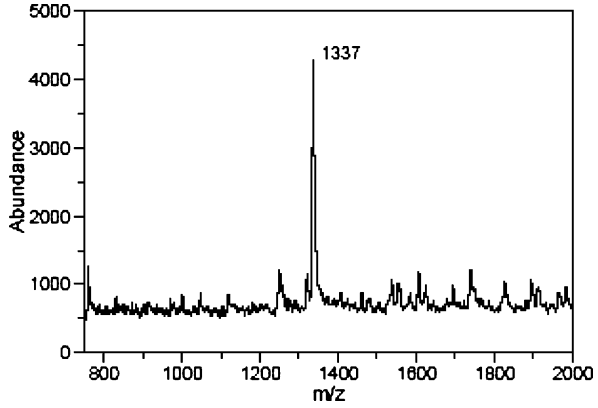

Figure 3. LDI-MS spectrum of **1H**, corresponding to the $[Mn_4O_2L^1_5]^+$ (butterfly) ion.

2; both the average Mn−(μ_3-O)(core) and Mn−O(L^1 or L^2) bonds in $\mathbf{1}^+$ and $\mathbf{2}^+$ are shorter by 0.025−0.047 Å than the corresponding values in **1** and **2**. The stronger Mn−O(L) phosphinate bonds and the stronger Mn−O(core) bonds will contribute a larger thermodynamic barrier to dissociation of the phosphinate anion and the O_2 product, respectively, thereby lowering the yield of the $Mn_4O_2L_5^+$ butterfly photoproduct in both oxidized cubanes, $\mathbf{1}^+$ and $\mathbf{2}^+$. Furthermore, because dissociation of a phosphinate anion (L^1 or L^2) is a prerequisite for O_2 release and butterfly formation, we can also expect a lower yield of the butterfly photoproduct for the oxidized cubanes, owing to the stronger attraction with the cationic charge of $\mathbf{1}^+$ and $\mathbf{2}^+$. Thus, both short-range bond strengths and long-range ionic attraction likely contribute to the lower yield of the butterfly photoproduct in the oxidized cubanes.

Because increasing the net charge of the core from $[Mn_4O_4]^{6+}$ to $[Mn_4O_4]^{7+}$ decreases the photodissociation yield of the "butterfly" as shown above, we might expect that decreasing the core charge should raise the yield of the butterfly photoproduct relative to the parent compound. This hypothesis was tested using the reduced cubane complex **1H** containing the $[Mn_4O_3OH]^{6+}$ core. The positive-ion LDI-MS spectrum of **1H** shows a single major peak with m/z = 1337 (Figure 3), corresponding to the $[Mn_4O_2L^1_5]^+$ (butterfly) ion. The parent ion for **1H** (m/z = 1587) is not observed using LDI, although **1H** is present as an intact molecular species in solution, as seen by electrospray ionization MS (ESI-MS; see the Supporting Information).[25] The LDI-MS result means that the photodissociation yield of the "butterfly" is extremely large in the gas phase, implying that one $Ph_2PO_2^-$ ligand and two core oxygen atoms in **1H** photodissociate with nearly 100% probability. The net charge of **1H** is the same as that of **1**, and thus local charge alone is not the major cause of the higher photodissociation yield. The higher yield of the butterfly photoproduct for **1H** in the gas phase correlates with both weaker Mn−O(core) and Mn−O(L^1) bonds, as is seen by FTIR spectroscopy; the symmetric O−P−O stretch is 993 cm^{-1}, larger than that of **1** (989 cm^{-1}), $\mathbf{1}^+$ (967 cm^{-1}), **2** (987 cm^{-1}), or $\mathbf{2}^+$ (964 cm^{-1}). Weaker Mn−O(L^1) bonding in **1H** is also evident by the greater lability of the $Ph_2PO_2^-$ anion to dissociation in solution phase, as measured by ESI-MS, which reveals a substantially greater fraction of $Mn_4O_4L^1_5{}^+$ (see the Supporting Information).[25]

DFT. To gain insight into the electronic factors governing the different photochemical and structural properties of complexes **1** and **2** and the corresponding cationic species $\mathbf{1}^+$ and $\mathbf{2}^+$, we performed DFT calculations. The highest occupied molecular orbital (HOMO) of **1** is composed of a degenerate pair of orbitals lying at −3.73 eV. The lowest unoccupied molecular orbital (LUMO) lies at −2.26 eV. Notice that, in *Gaussian03*, calculations under T_d symmetry are actually performed in D_2 symmetry, which does not contain degenerate representations. The degenerate HOMOs and the LUMO all belong to the t_2 representation in T_d symmetry. The three t_2 partners split in D_2 symmetry into two almost perfectly degenerate singly occupied orbitals and one unoccupied orbital, with the energies of the HOMOs and of the LUMO differing because of the different occupation numbers of the three orbitals.

Inspection of the frontier orbitals of complex **1** shows that the HOMOs are made by combinations of manganese d_{z^2} orbitals involving the four manganese atoms, mixed in an antibonding fashion with O lone pairs from both the core (O) and the phosphinate (O′) ligands; see Figure 4. The two degenerate HOMOs and the LUMO have the same orbital character but different spatial orientations. The population of these degenerate HOMOs with two electrons and their manganese−oxygen antibonding character is responsible for the unusually long Mn−O and Mn−O′ distances found in complex **1**. Moreover, we can readily understand the increased quantum yield for release of a phosphinate ligand from **1** with respect to $\mathbf{1}^+$; indeed, upon oxidation of **1** to $\mathbf{1}^+$, an electron is expelled from the degenerate HOMO pair, thus reducing the antibonding interaction and resulting in stronger Mn−O bonds. This prediction is supported by the results of a separate calculation performed on $\mathbf{1}^+$ at the optimized geometry of **1**, showing that the HOMO is a singly occupied orbital having the same character as that in **1**.

For complex **2**, we calculate an electronic structure qualitatively similar to that of complex **1**, with a degenerate HOMO contributing antibonding character to all Mn−O and Mn−O′ bonds. Notably, however, for complex **2**, the HOMOs are calculated to be considerably destabilized with respect to **1**, now lying at −2.98 eV, which is 0.75 eV higher in energy than the HOMOs of complex **1**. This behavior is due solely to the increased donor ability of the $(H_3CO-Ph_2)PO_2^-$ ligand with respect to the $Ph_2PO_2^-$ ligand because vibronic distortions were excluded by constraining the geometry to that calculated for **1**. Similar to complexes **1** and $\mathbf{1}^+$, the reduced quantum yield observed for $\mathbf{2}^+$ with respect to **2** is related to depopulation of the antibonding HOMOs upon one-electron oxidation of the neutral complex.

The higher energy of the HOMO calculated in complex **2** (weaker electron binding) reveals an overall destabilization of this complex with respect to **1**, which should, in turn, translate to a further weakening of the Mn−O and Mn−O′ bonds. The picture derived from the electronic structure is supported by the calculated LBE, showing for complex **2** an LBE that is 14.7 kcal/mol lower than that for complex **1**.

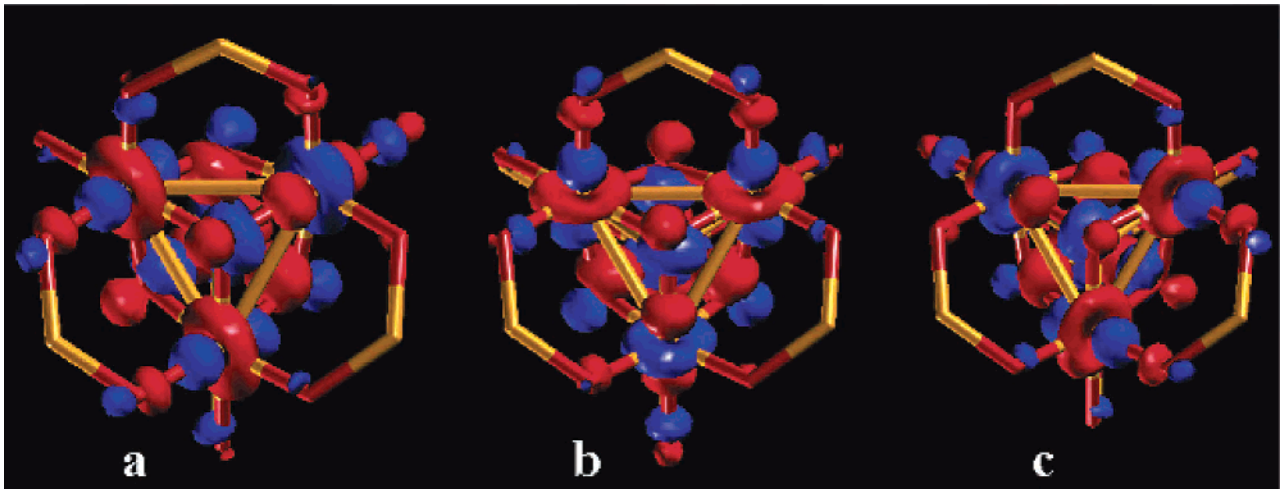

Figure 4. Isodensity plot of the degenerate HOMO pair (a and b) and of the LUMO (c) of **1**. Isodensity value = 0.04. Phenyl rings have been omitted for clarity.

Even though this value might vary weakly upon allowing for geometry relaxation, the quite high difference between the LBE in complexes **1** and **2** readily supports the experimental results, showing an increased quantum yield for ligand photodissociation from **2**.

Conclusions

It is significant that complex **2** produces a much higher yield of the ligand photodissociation product than does **1** in the gas phase. This result is also true for $\mathbf{2}^+$ versus $\mathbf{1}^+$, although not nearly so large an increase. The appreciably lower calculated LBE (14.7 kcal/mol) in the ground state for the L^2 phosphinate in **2** than that of L^1 in **1** is a principal source of this difference in the photodissociation yield. The electronic structure calculations show that greater electron donation by L^2 versus L^1 and the antibonding nature of the HOMOs of complexes **1** and **2** provide a self-consistent quantitative rationale for this trend in the photodissociation yield. These electronic properties also account well for the 150-mV downshift of the $\mathbf{2}^+/\mathbf{2}$ reduction couple relative to $\mathbf{1}^+/\mathbf{1}$.[24] These observations are also qualitatively accounted for by the empirical π-electron donation properties of the *p*-CH_3O group in homologous substituted phenyl compounds.[34]

Although **2** shows a higher photodissociation yield than **1** in the gas phase, neither exhibits appreciable photochemistry in the condensed phase. The absorption spectra of solutions of **2** and $\mathbf{2}^+$ in CH_2Cl_2 or CH_3CN do not change under continuous illumination in the UV−vis region (xenon lamp, from 190 nm to near-IR). This result was also confirmed by MS. This lack of photoreactivity in solution is the same as that observed for **1**,[22,23] most probably because of efficient quenching of the excited state or rapid geminate recombination of L^- and $L_5Mn_4O_4^+$ in the solvent cage. The increasing yield of the butterfly photoproduct (and dioxygen) in the gas phase upon decreasing the core oxidation and by eliminating the formal 1+ charge from $Mn_4O_4^{7+}$ to $Mn_4O_4^{6+}$ is opposite to that of the natural PSII WOC system, which yields O_2 only in the highest (S_4) oxidation state. The final concerted step of the PSII WOC catalytic cycle, $2H_2O + S_4 \rightarrow S_0 + O_2 + 2H^+$, is thought to be induced by increasing the formal Mn_4 oxidation state via PCET to the PSII reaction center (not direct photochemistry of Mn) and is coupled to a core structural change involving product release and substrate water rebinding.[11,26] This difference suggests that the high kinetic barrier to O_2 production by the Mn−oxo "cubane" core molecules in the gas phase, versus the lower barrier for the natural PSII WOC, may have two sources. First, the requirement to dissociate a phosphinate anion implies the existence of an unstable photointermediate (peroxo?, Scheme 1) that precedes the release of O_2 and decays back to the unaltered cubane ground state as a result of geminate recombination in solution. Second, the presence of water is likely important to favor the displacement of O_2 by coordination to reduced Mn ions in the coordinatively unsaturated $[Mn_4O_2L_5]^+$ butterfly core product.

In summary, variation of the capping ligand and core oxidation state does modify appreciably the photochemical yield of oxygen release from the manganese−oxo cubane complexes $[Mn_4O_4L_6]^{0/+/-}$ in the gas phase. Stronger electron-donating phosphinate derivatives are found to increase the yield of photoproduct and to lead to a wider range of minor photoproducts. However, this change does not improve the photodissociation yield of the butterfly product in the condensed phase, where the barrier to O_2 release remains too high to overcome for the Mn_4O_4 cubane topology. Thus, to achieve catalytic water oxidation using Mn−oxo cubanes, other approaches will have to be explored to lower the barrier to ligand dissociation as a precursor to the release of O_2 in solution. One possible contribution to lowering the kinetic barrier to intramolecular O_2 release to consider in future studies should involve the influence of Ca^{2+} replacing Mn^{3+} within the $Mn_4O_4L_6$ core. This replacement should provide further insight into the possible role of calcium in the photosynthetic enzyme.[6,10,11,20,35]

(34) Hammett, L. *Physical organic chemistry; reaction rates, equilibria, and mechanisms*; McGraw-Hill: New York, 1940.

(35) Messinger, J. *Phys. Chem. Chem. Phys.* **2004**, *6*, 4764.

Acknowledgment. This research was supported by the National Institutes of Health (Grant GM-39932). J.-Z.W. is grateful to the China Scholarship Council for partial fellowship support. Drs. John Eng and Dorothy Little are acknowledged for their help in MS measurements. We thank Dr. Alexei M. Tyryshkin for help with EPR measurements.

Supporting Information Available: CIF file, ^{1}H NMR, FTIR, UV−vis, LDI-MS, and EPR spectra of $\mathbf{2}^+(ClO_4^-)$, and ESI-MS spectra of **1H**. This material is available free of charge via the Internet at http://pubs.acs.org.

IC051587R